An Improved Magnetic-Geared Permanent Magnet In-Wheel Motor for Electric Vehicles

Ying Fan, Hehe Jiang, Ming cheng, Yubin Wang
School of Electrical Engineering，Southeast University，Nanjing, China, 210096
E-mail: vickifan@seu.edu.cn; 309260345@qq.com; mcheng@seu.edu.cn; yubwang5190@163.com

***Abstract*-This paper introduces an improved magnetic-geared permanent magnet (MGPM) in-wheel motor with high power density and torque density for electric vehicles (EVs). Due to the integrating of the magnetic gear and omitting of the gear inner rotor, the motor can achieve the low speed direct driving and high speed compact designing requirements with even simple structure. The principle and optimized structure are described. A 750w optimized motor is designed and analyzed by finite element method. The simulation results validate that the MGPM in-wheel motor can be operated at low speed, high efficiency and high torque. It is suitable for direct-driving EVs.**

***Index Terms* — EVs; Magnetic gear; Permanent magnet; In-wheel motor**

I. INTRODUCTION

With ever growing energy crisis and environment degradation, there are more and more concerns with the electric vehicles (EVs). Motor is the important part of EVs, growing interests are taken for in-wheel motor, it has a lot of potential benefits [1-2]. As the wheel motor of the EVs is designed either as a permanent magnet (PM) brushless gearless outer-rotor or a high speed planetary-geared inner-rotor one, both of the two structures have some disadvantages. The former is no gear, it is bulky and heavy because it should operate at low speed. The second takes the advantages of smaller size and weight, but the needing of mechanical gearbox which means inevitably transmission loss, acoustic noise and lubrication.

Recently, the conception of magnetic gear has been paid much attention. It can offer high torque density comparable to mechanical gearboxes that has some distinct advantages [3]. Researches indicate that the coaxial topology of the magnetic gear will greatly improve the utilization of PMs [4]. Through integrating a coaxial magnetic gear into a PM brushless motor, the low-speed requirement for direct driving and the high-speed requirement for motor design can be achieved simultaneously [5]. Fig. 1 shows the configuration of the former proposed magnetic-geared PM in-wheel motor. The motor includes four main parts: the stator, the outer rotor, the stationary ring and the gear outer rotor. The tire rim is directly mounted onto the gear outer rotor. With this structure, the torque density and reliability can be significantly improved. However, this compacted structure is more or less bulky and the installation is complex. On account of this disadvantage, a simplified motor is designed [6], in which a stationary armature is employed to replace the inner high-speed rotor of the magnetic gear. Fig. 2 is the topology of this motor. In this paper, an improved magnetic-geared PM motor is proposed, on which the tire is directly mounted. Simulation results show that the performance is suitable for EVs. Some optimization has also been made. A 750w optimized motor will be analyzed to validate the proposed in-wheel motor.

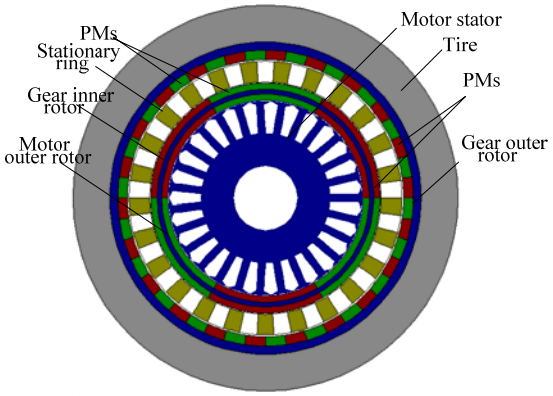

Fig. 1. Configuration of the magnetic-geared PM in-wheel motor with three air-gap [5].

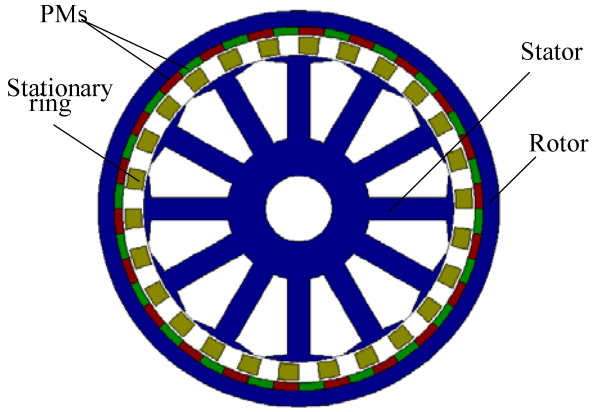

Fig. 2. Configuration of the magnetic-geared PM brushless motor with two air-gap [6].

II. MOTOR TOPOLOGY and OPERATION PRINCIPLE

A. *Motor Topology*

Fig. 3 shows the topology of the proposed in-wheel motor for EVs, in which the tire rim is directly mounted onto the motor outer rotor. The motor has 23 pole pairs of rotor, 27 pole pairs of stationary ring and 18 slots. This in-wheel motor adopts an improved rotor that the PMs are buried in the iron

978-1-4244-8218-4/10/$26.00 ©2010 IEEE

core of the rotor and magnetized in the same direction. This motor can reduce the material of the PMs, iron loss and also eddy current loss.

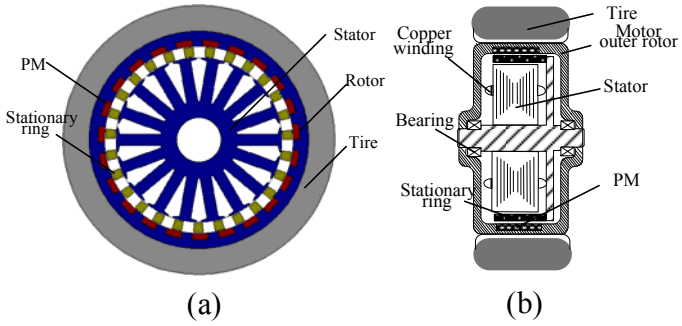

Fig. 3. Configuration of the proposed in-wheel PM motor. (a) Front view (b) Side view.

B. *Motor Principle*

The key of the operation principle is the flux modulation function of the stationary ring which is the middle part of the traditional magnetic gear. The inner rotor of the magnetic gear is omitted. So the motor has two air-gaps. The magnetic field created by the inner rotor of the traditional magnetic gear is substituted by the stator winding. When the machine is operating as a motor, the windings are fed current with certain frequency. A rotating magnetic field with the speed ω_1 is produced in the air-gap near the stator, with the stationary ring modulating function, a harmonic rotating magnetic field is produced in the air gap near the rotor. Its speed is $-\omega_2$ (minus means the opposite rotating direction of the two kinds of magnetic field). The outer rotor rotates with the interaction of the outer air-gap field and the permanent magnet of the rotor.

According to [3], in order to utilize the maximum harmonic field and transmit a steady torque the number of pole pairs of the outer rotor p_r should be equal to p_m minus p_s. So the speed ratio G_r is given in (1)

$$G_r = \frac{\omega_2}{\omega_1} = \frac{|P_s - P_m|}{P_s} \tag{1}$$

where p_s is the number of pole pairs of the stator field, and p_m is the number of the pole pairs of the stationary ring.

According to [4], the ratio 5.75:1 of the magnetic gear, with p_s=4, p_r=23 and p_m=27 exhibits a virtually ripple-free and high torque transmission capacity, for motor operation, this type of matching is suitable for in-wheel motor.

III. Optimization of Motor Parameters

The proposed motor with the number of pole pairs of rotor and stationary ring fixed, the slot number of the stator, width of the modulation block in the stationary ring and width of PMs are variable parameters that should be discussed [7].

A. *Choice of the Slot Number*

As it is well known, different slot number of different options has some influence for the winding connections and cogging torque. The common multiple is large of the motor rotor and the stationary ring pole pairs; therefore the cogging torque is small. But the slot number will influence the winding connection that the winding package factor will be changed for different slot numbers. Here, three types of the slot number with 12, 18 and 27 are investigated by finite element method (FEM). In order to compare these three different choices, the same stator outer dimension, slot package factor, slot depth and material are taken. The principles of winding connection are to produce the maximum back EMF and achieve p_s = 4. Thus, concentrated doubled-layer windings are adopted for the 12-slot stator; fractional distributed doubled windings are employed for 18- and 27- slot stators respectively. Fig. 4 shows the back EMF based on these three kinds of slot. It can be noted that the fractional distribution winding is better than the concentrated winging as the winding package factor increased. But more slots will lead to increase the manufacturing complexity. To make a compromise, the use of 18 stator slots is adopted.

Fig. 5 shows the 18-slot stator winding connection of the proposed machine. It adopts three-phase symmetric distributed windings of 18 double-layer coils.

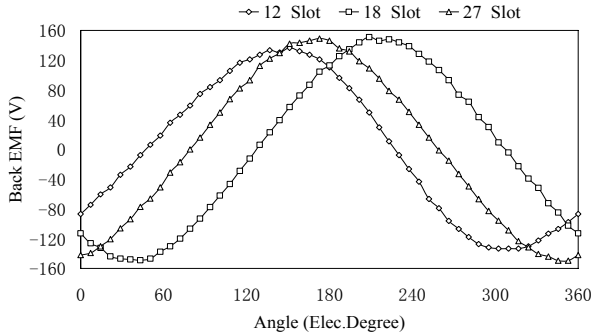

Fig. 4. Back EMF waveforms with three different slot numbers.

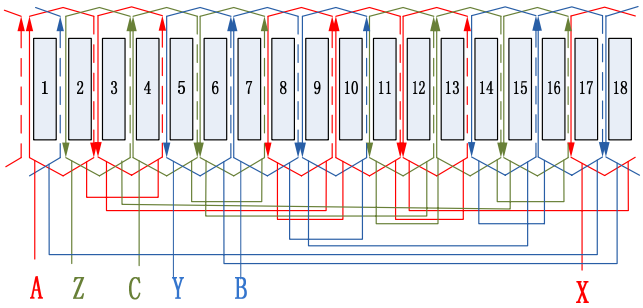

Fig. 5. Stator winding connection of the proposed motor.

B. *Stationary Ring Optimization*

The stationary ring is built of laminated ferromagnetic materials which provide the path for magnetic field, the remained parts of the stationary ring is epoxy which can't lead field. These two parts distributed in interval method along the circumference. The function of the modulation blocks on the stationary ring is to modulate the air-gap field space harmonics. Changing the width of the modulation blocks will not change the motor total volume but the

magnetic fields of the two air-gaps which relate to the energy transmission. Due to this, impaction on the highest steady torque created by different width of the modulation block is analyzed. In order to change the width by some regularity, the width 360 /2 p_s is used as the based width and the ratio of the modulation block width is taken as a variable parameter. The relationship between this ratio and the maximum static torque is presented in Fig. 6. From this figure, when the ratio equals 0.9, the maximum static torque is achieved.

C. Rotor Optimization

Due to the special rotor structure that the permanent magnetics (PMs) is magnetized in the same direction, the width of the PMs should properly choose to achieve the optimum performance. With the width of the PMs increasing, the motor back EMF is enhanced. When the width of PMs increases to a certain value, the back EMF produced by per unit PMs will not be increased, the based width is the equal spaced one. When changing the width of the PMs, the back EMF also changes.

By comparing the maximum value of the back EMF, the best width of the PM can be confirmed. Fig. 7 shows the relationship between the ratio and the maximum value of the back EMF. From the figure, we choose 1.2 to achieve the better and economical performance.

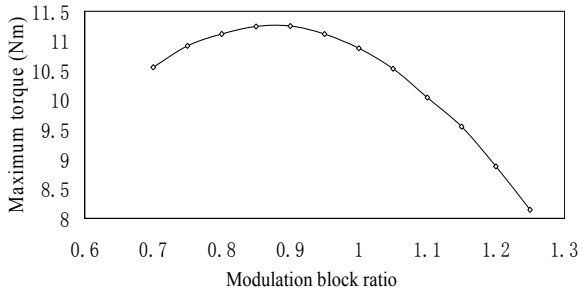

Fig. 6. Maximum torque at different width ratios of the modulation block.

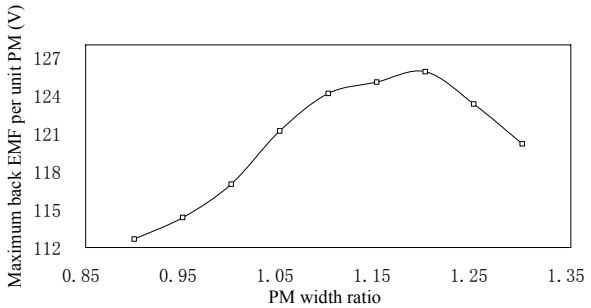

Fig. 7. Relationship between the PM width ratio and the maximum back EMF.

IV. Simulation of the Optimized Motor

The specifications of the optimized machine are listed in Table Ⅰ. The 2-D finite element analysis (FEA) model is employed to analyze the static characteristics of the optimized motor.

A. No-load Flux Density Distribution

Fig. 8 is the no-load magnetic field distribution. It can be noted that most part of the flux lines which produced by the outer rotor PMs pass through the modulation blocks of the stationary ring. This indicates that the stationary ring can affect the magnetic field. Also from the figure, the flux lines in the stator core denote that the pole pair number is four.

Fig. 9 shows the radial flux density waveforms inside and outside surface of stationary ring built up by the rotor. To further validate the stationary ring modulation function, the harmonics of the two air-gap magnetic fields are analyzed. Fig. 10 is the radial magnetic field harmonic analysis of the air-gaps fields. It shows that the magnetic field mainly pole pair number is four of the inner air-gap, while the outer air-gap is 23. Therefore due to the stationary ring, the magnetic field is changed from 23 of the outer air-gap to 4 of the inner air-gap. The speed variation of the two air-gaps magnetic fields is achieved; the magnetic gear speed changing is realized.

TABLE I.
SPECIFICATIONS OF PROPOSED MOTOR

Item	***Value***
Rotor pole-pair number	23
Stationary pole-pair number	27
Stator slot number	18
Rated frequency	230Hz
Rated speed of motor outer rotor	600 rpm
Rated phase voltage	110V
Rated power	750w
Radius of house	74.5 mm
Air-gap length	0.6 mm
Thickness of PMs	4.5 mm
Thickness of stationary ring	6.5 mm
Inner radius of rotor	64 mm
Motor active axial length	32 mm
Remanence of PMs	1.2 T
Modulation block width ratio	0. 9
PM width ratio	1. 2
Number of winding turns per coil	90

B. Back EMF Calculation of the Optimized Motor

Fig. 11 shows the back EMF waveforms of the optimized motor with the rotor rotating at a certain simulation step in one electric cycle. The flux linkage is obtained by the simulation results. The back EMF can be calculated as (2)

$$e = \frac{d\psi}{dt} = \frac{d\psi}{d\theta}\cdot\frac{d\theta}{dt} = \frac{d\psi}{d\theta}\cdot\frac{2n\pi}{60} = d\psi\cdot\frac{180}{\pi\cdot d\theta}\cdot\frac{2n\pi}{60} = d\psi\cdot\frac{6n}{d\theta} \quad (2)$$

where θ is the simulation step length, n is the rated speed of the rotor.

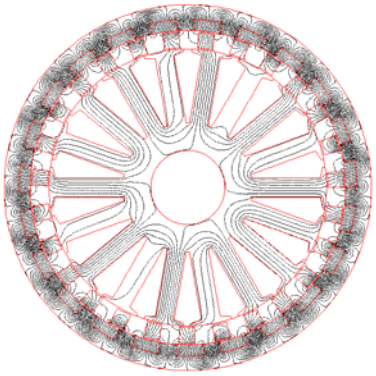

Fig. 8. No-load magnetic field distribution.

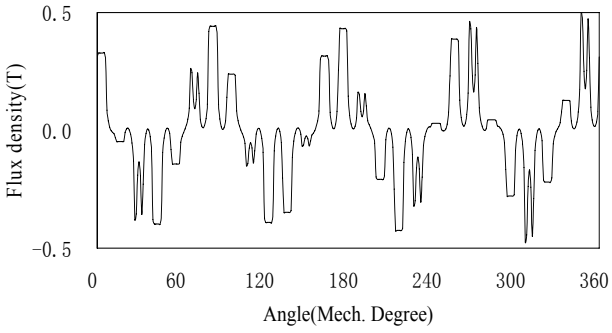

(a)

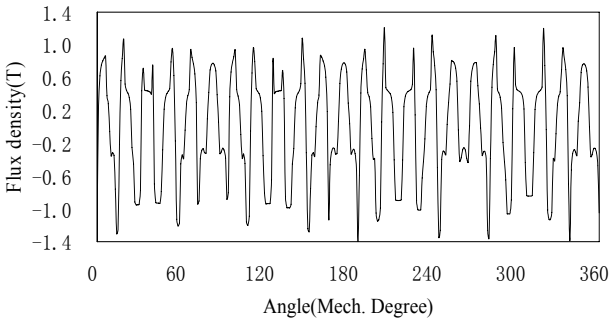

(b)

Fig. 9. Radial magnetic field waveforms of the air-gap. (a) inner air-gap (b) outer air-gap

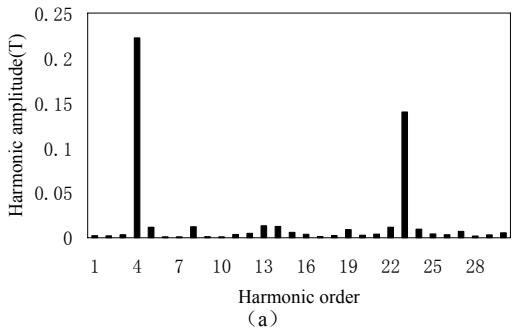

（a）

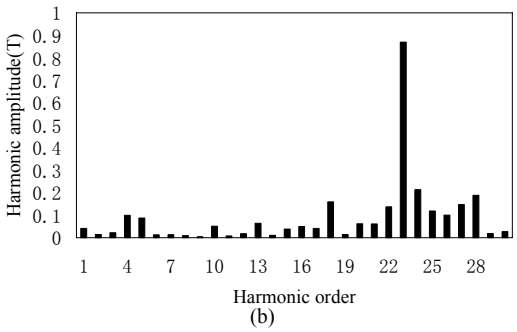

(b)

Fig. 10. Radial magnetic field harmonic analysis of the air-gap' fields. (a) inner air-gap (b) outer air-gap.

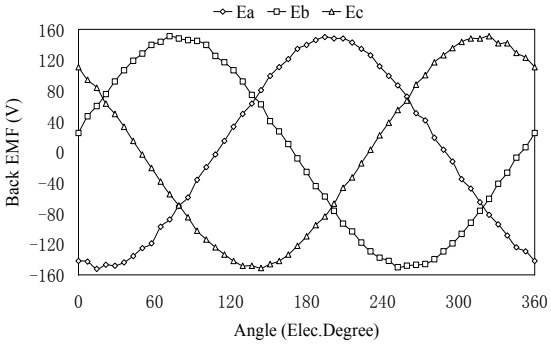

Fig. 11. Back EMF waveforms .

C. Steady Torque Calculation of the Optimized Motor

To obtain the rated output torque, 3-phase symmetric currents synchronized with the same phase of back EMF are fed into the windings. The output torque in an electric cycle is shown in Fig. 12. The torque ripple is small which is caused by cogging torque. Fig. 13 shows that the cogging torque is very small. This is because the common multiple of the pole pair number and the stationary ring pole pair number is quite large.

Fig. 12. Output torque waveform.

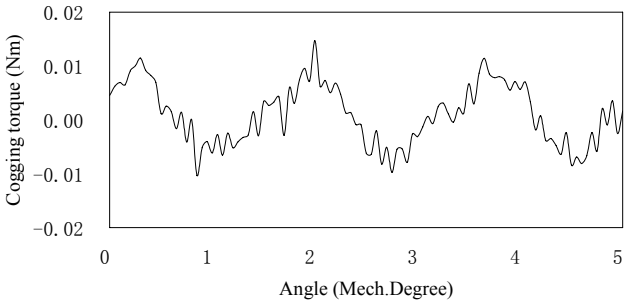

Fig. 13. Cogging torque waveform.

V. Conclusion

In this paper, a magnetic-geared PM motor with tire directly mounted is designed. The low-speed requirement for direct driving and the high-speed requirement for motor design can be achieved simultaneously through an improved magnetic gear which the inner rotor is omitted. Optimization has been made to fix some motor parameters. A two-dimensional FEM model is established to analyze the static characteristics of the motor. Simulation results validate that the motor can be operated at low speed, high torque and high efficiency. It is suitable for the EVs with simple structure.

Acknowledgment

This work is supported and funded by the funding (Project No. 50729702) from the National Natural Science Foundation of China, by the funding from the Chang Jiang Chair Professorship at Southeast University, Nanjing, and the funding (Project No. BE 2008130) from the Key Technology R&D Program of Jiangsu Province, China.

References

[1] H. Shimizu, J. Harada. C. Bland. K. Kawakami, L. Chan, "Advanced concepts in EV design," IEEE Trans. Ind. Electron., vol. 44, no. 1, pp. 14-18, Feb. 1997.

[2] C. C. Chan and K. T. Chau, "Modern Electric Vehicle Technology," Oxford University Press. 2001.

[3] K. Atallah and D. Howe, "A novel high performance magnetic gear," IEEE Trans. Magn., vol. 37, no. 4, pp. 2844-2846, Jul. 2001.

[4] K. Atallah, S. D. Calverley, and D. Howe, "Design, analysis and realisation of a high-performance magnetic gear," IEE Proc.-Electr. Power Appl.,vol. 151, no. 2, pp. 135-143, Mar. 2004.

[5] Linni Jian, K. T. Chau, and J. Z. Jiang, " An integrated magnetic-geared permanent- magnetic in- wheel motor drive for electric vehicles," IEEE Vehicle Power and Propulsion Conference, 2008.

[6] Michal-Wolfgang Waszak, Jan Hemmelmann, Ronghai Qu, and Patrick Lee Jansen, "Electric machine apparatus with integrated, high torque density magnetic gearing," U. S. patent 0186692, Aug. 16, 2007.

[7] P. O. Rasmussen, T. M. Jahns and H. A. Toliyat, "Motor integrated permanent magnet gear with a wide torque-speed range," Energy Conversion Congress and Exposition, 2009, ECCE 2009. IEEE, pp. 1510-1518.